The Effects of Heat Transfer in Melt Spinning

R. E. MAEBIUS, *PPG Industries, Inc., Fiber Glass Research Center, P.O. Box 2844, Pittsburgh, Pennsylvania 15230*

Synopsis

Several heat transfer models are examined in order to assess the influence of convection and radiation upon the melt spinning of a Newtonian fluid. In the spinning of glass fibers, radiation is shown to be equally as important a mode of heat transfer as convection. Small changes in the spectral emissivity are shown to have a large effect on the shape of the jet and the drawing force required to attenuate the fiber.

INTRODUCTION

Melt spinning is the manufacturing technique used in the production of synthetic and glass fibers. In this process, a liquid melt is drawn from a small tip or spinnerette and attenuated into a fiber of desired diameter. During the attenuation process, the fiber is rapidly cooled. If, as in some cases, the viscosity is a strong function of temperature, a rapid increase in the viscosity takes place. For the case of glass, as the fiber nears its glass transition temperature, viscoelastic effects may become important.

Since cooling has such a strong influence on viscosity during the attenuation, heat transfer is a very important mechanism governing the production process.

Up to this point, there appears to have been very little information published in the literature which assesses the effect that different heat transfer models have upon the process.

There are two modes of heat transfer that must be considered. These are convection and radiation.

In this article, several heat transfer models are examined in order to assess the influence of convective heat transfer and radiative cooling in the melt spinning of glass fibers. Many approaches to estimate the value of the convective film transfer coefficient have been used in previous works. Glicksman[1] used a Reynolds analogy[2] based on the work of Glauert and Lighthill[3] to estimate the value of the local film coefficient. The Reynolds analogy assumes that the air Prandtl number is unity. This assumption requires that the thickness of the momentum and thermal boundary layers surrounding the glass strand be equal. Glauert and Lighthill assumed that the momentum boundary layer was developed from the leading edge of a fixed, infinitely long cylinder. They derived their results based on a series solution for the boundary layer using the Von Karman–Pohlhausen technique.[2] Sakiadis[4] also used this technique; however, he employed a different velocity profile in order to match the momentum boundary conditions in his problem. Unlike Glauert and Lighthill's formulation, Sakiadis assumed that the boundary layer was developed from the point where an infinite

Journal of Applied Polymer Science, Vol. 30, 1639–1652 (1985)
 CCC 0021-8995/85/041639-14$04.00

cylinder was issued from a wall at constant velocity through a surrounding medium that would otherwise be at rest.

Glauert and Lighthill's and Sakiadis' work were both theoretical in nature and considered the case of a constant diameter cylinder moving at constant velocity. More recently Sayles,[5] who cites the work of Moore and Pearson,[6] introduced a formulation that took into account the curvature of the fiber and showed that the effects of curvature may increase the value of the local Nusselt number by as much as 28%. Sayles did not attempt to develop the energy equation for the thermal boundary layer however and resorted to a Reynolds analogy in order to estimate the film coefficient.

Bourne and Elliston[7] also used the Von Karman–Pohlhausen technique to study the development of the momentum and thermal boundary layers of a constant diameter fiber. Their formulation introduced a correction factor to account for Prandtl numbers less than unity. The calculated results they obtained for the Nusselt number tended to underpredict the experimental data available to them by about 8%. Other authors have used different techniques to study the effect of heat transfer. Geyling,[8] in his linear stability analysis, assumed a constant film coefficient (constant Stanton number) in order to assess the effects of the Reynolds, Weber, and Froude numbers on jet stability.

Since it was not the goal of this investigation to develop either a theoretical or empirical model to evaluate the convective film coefficient, information available from the open literature was used in order to assess the effects of different heat transfer correlations on the glass forming process. A comparison of the effects obtained by using different heat transfer models will enable us to establish the influence that these models will have on the filament diameter and drawing force.

According to White,[9] the most generally accepted correlation for a moving fiber was developed by Kase and Matsuo.[10] Their correlation was given in the form

$$\mathrm{Nu} = hd/K_a = 0.42(\mathrm{Re}_a)^{0.344} \tag{1}$$

where Nu is the local Nusselt number, Re_a, the local Reynolds number based on the air kinematic viscosity, local fiber diameter, and velocity, h, the local film coefficient, d, the local fiber diameter, and K_a, the thermal conductivity of air. Kase and Matsuo[10] developed their correlation based on data they obtained by subjecting a 0.2 mm diameter heated wire to airflow both parallel and at right angles to the wire for values of Re_a in the range of 0.5–50.

Kase and Matsuo[11] later extended their results to represent the presence of cross flow more accurately; however, these effects are not considered in this paper.

Other authors[12–14] have investigated the effects of air drag on single filaments and have derived empirical correlations for the skin friction coefficient C_f of the form:

$$C_f = \alpha(\mathrm{Re}_a)^{\beta} \tag{2}$$

where α and β are experimentally determined constants. The values of α and β reported in Ref. 12, 13, and 14 are shown in Table I.

Both the Sano–Orii[12] and Hamana et al.[13] correlations are based on fibers of diameters 30–100 μm moving at velocities between 200 and 1200 m/min. A later paper by Matsui[15] shows that the coefficients in Ref. 13 are valid up to 6000 m/min. Matsui obtained his data by using a Rothschild tensiometer to measure the increase in drawing force of polyester filaments spun from a spinnerette after the elongational deformation was completed. The final diameter of the solid filaments ranged from 29 to 86 μm.

Gould and Smith[14] evaluated data for fibers less than 300 μm at speeds up to 6000 m/min. They obtained their data by suspending filaments from a strain gauge inside a specially constructed wind tunnel. They also reanalyzed the data of Sano and Orii[12] by performing a least-squares linear regression analysis. Gould and Smith showed that the original data collected by Sano and Orii would be best represented if the parameter estimates of 0.68 and -0.80 for α and β where replaced by 0.42 and -0.64, respectively. It is interesting to note that their revised estimate of -0.64 for β is very close to the value they calculated in their own study and the value reported by Hamana et al.[13] They also found that fibers of the order of 10–100 μm in diameter were not affected by air drag due to neighboring filaments unless the spacing between them was less than 1 mm.[13]

In this study, both the Reynolds and Chilton–Colburn[16] analogies have been used to estimate the local Nusselt number using the skin friction correlations shown in Table I.

In the Reynolds analogy, the Stanton number, St, is directly related to the skin friction coefficient as

$$\mathrm{St} = \frac{\mathrm{Nu}}{\mathrm{Re\ Pr}} = \frac{1}{2}C_f \tag{3}$$

where Pr is the air Prandtl number. It is also assumed that the Prandtl number for air is equal to unity. Notice that rearranging eq. (3) by multiplying through by Re_a yields an exponent parameter of 0.39 for both the Gould–Smith and Hamana et al. correlations which is very close to the value quoted by Kase and Matsuo of 0.334, the leading coefficients being slightly smaller.

In the Chilton–Colburn analogy,[16] the effect of Prandtl numbers less than unity can be accounted for as follows:

$$\mathrm{St} = \frac{1}{2}C_f\,\mathrm{Pr}^{-2/3} = \frac{\mathrm{Nu}}{\mathrm{Re\ Pr}} \tag{4}$$

TABLE I
Skin Friction Parameters for Single Filaments

Author	α	β
Sano–Orii[12]	0.68	-0.80
Hamana et al.[13]	0.37	-0.61
Gould–Smith[14]	0.41	-0.61

Thus, the expression for the local Nusselt number becomes

$$\mathrm{Nu} = \frac{1}{2} C_f \,\mathrm{Re}\,\mathrm{Pr}^{1/3} \tag{5}$$

The Chilton–Colburn analogy is valid for values of the Prandtl number in the range $0.60 < \mathrm{Pr} < 60$. For air at 1000°F and atmospheric pressure, the value of Pr as determined from Eckert and Drake[17] is 0.6895 which is within the limits of the validity of the Chilton–Colburn analogy.

ANALYSIS

In the calculations reported here, a 1-dimensional model of a Newtonian fluid has been employed to study the effects convection and radiation. This approach is well established and has been widely used in the literature.[18–20] As Denn[20] and several other investigators have noted, the 1-dimensionality assumption is based on the small-slope approximation which requires that the curvature of the fiber in the axial direction be very small ($dr/dz << 1$). This breaks down near the tip or spinnerette where the curvature may be large and a more complex, 2-dimensional analysis may be needed there. It is, nevertheless, still worth pursuing the 1-dimensional analysis, keeping in mind the restriction imposed by the small-slope approximation.

Using cylindrical-polar coordinates and assuming steady-state axisymmetric flow, the governing equations can be written as[21]

$$\pi r^2 v = Q_0 \tag{6}$$

$$\rho v \frac{dv}{dz} = \frac{6\mu}{r}\frac{dv}{dz}\frac{dr}{dz} + \frac{d}{dz}\left(3\mu \frac{dv}{dz} - \frac{\gamma}{r}\right) + \rho g \tag{7}$$

$$\rho C_p v \frac{dt}{dz} = -\frac{2h}{r}(T - T_a) - \frac{2\epsilon\sigma}{r}(T^4 - T_a^4) \tag{8}$$

where Q_0 is the volumetric flow rate, ρ the density, μ the dynamic viscosity, γ the surface tension, g the gravity, v the axial fiber velocity, r the local fiber radius; T the local fiber temperature, T_a the environment temperature, C_p the specific heat at constant pressure, h the film transfer coefficient, ϵ the hemispherical emissivity, and σ the Stefan–Boltzman constant.

Equations (6)–(8) represent the continuity, momentum, and energy equations. Note that in the formulation of the momentum equation, the effect of air drag has been neglected.

In all the calculations reported here a glass whose viscosity can be expressed by the Vogel relationship has been employed and is given approximately as

$$\log \mu = 4900/(T - 1000) - 1.2 \tag{9}$$

Other parameters used in the calculations are shown in Table II.

Several calculations were made in order to assess the influence of the different convective film transfer models upon the shape of the jet and the drawing force. A fixed ambient temperature of 1000°F and a spectral em-

TABLE II

Flow rate	0.005	g/s
Final strand velocity	200.0	ft/s
Density	159.19	lbm/ft^3
Specific heat	0.36	BTU/lbm · °F
Surface tension	330.0	dyn/cm
Thermal conductivity	16.69	BTU/h · ft · °F

issivity of 0.30 were used and assumed to be constant. An initial temperature of 2100°F was assumed to be the temperature of the glass at the orifice exit.

A spatially accurate fourth-order Runge–Kutta method[22] was used to obtain the solution of the governing equations in all of the calculations.

The convection models chosen for study in this analysis were: (1) constant film transfer coefficient; (2) Kase–Matsuo correlation[10]; (3) Sano–Orii correlation[12]; (4) Hamana–Matsui–Kato correlation[13]; and (5) Gould–Smith correlation.[14]

For the case of a constant film coefficient, a value $h = 10$ BTU/h · ft^2 · °F was used. It should also be remembered that the Gould–Smith, Hamana et al., and Sano–Orii correlations are not strictly heat transfer models since they are based on assumptions regarding the similarity of the momentum and thermal boundary layers surrounding the fiber.

All of the above models were evaluated with and without radiation. In another calculation all effects of convection were eliminated by setting $h = 0$ and the solution was obtained using radiation as the only mode of cooling.

In all cases, the average Nusselt number was calculated as

$$\langle \mathrm{Nu} \rangle = \frac{1}{L} \int_0^L \mathrm{Nu}\, dz \tag{10}$$

and the average film coefficient was calculated as

$$\langle h \rangle = \frac{1}{L} \int_0^L \frac{\mathrm{Nu}\, K_a}{2r}\, dz \tag{11}$$

where Nu, r, and K_a are the local Nusselt number, local fiber radius, and thermal conductivity of air. Equations (10) and (11) were integrated numerically using a second-order accurate trapezoidal integration method.

The drawing force required to attenuate the fiber was calculated using a linear momentum balance. The control volume was taken to include the fiber from the point at which the melt left the spinnerette up to the location where it achieved its final radius and velocity. Air drag was neglected.

RESULTS AND DISCUSSION

The Effects of Convection

Figures 1 and 2 show the results obtained with the three-skin friction correlations shown in Table I using both the Reynolds and Chilton–Colburn

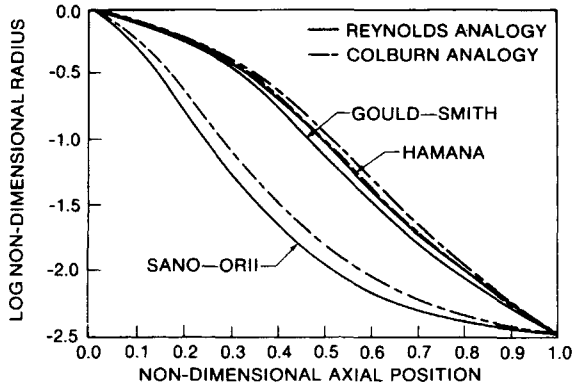

Fig. 1. Log nondimensional fiber radius vs. nondimensional axial position: (—) Reynolds analogy; (– -) Colburn analogy.

analogies in the absence of radiation. Figures 1 and 2 present the shape and temperature profile of the jet. Notice that the results obtained using both the Gould–Smith and Hamana et al. correlations are very similar. This is because of the common exponential factor of -0.61 in eq. (1). Since the leading coefficient of 0.37 in the Hamana et al. correlation is smaller than the value of 0.41 reported by Gould and Smith, the Hamana correlation leads to a slightly smaller value of the local Nusselt number.

These correlations both predict a smaller film transfer coefficient than the one calculated by the Sano–Orii correlation. In these calculations, the original parameter estimates of α and β as reported by Sano and Orii and shown in Table I have been used. If, instead, the values of 0.42 and -0.64 calculated by Gould and Smith[12] to correlate the Sano–Orii data had been employed, we would expect to see results that differ little from those calculated using the Gould–Smith and Hamana et al. correlations. This is due to similarity of the parameter estimates.

The solid lines in Figures 1 and 2 represent the effect of using the Reynolds analogy. The Chilton–Colburn analogy results are shown by the dotted lines. Since the Chilton–Colburn analogy includes the effects of the Prandtl num-

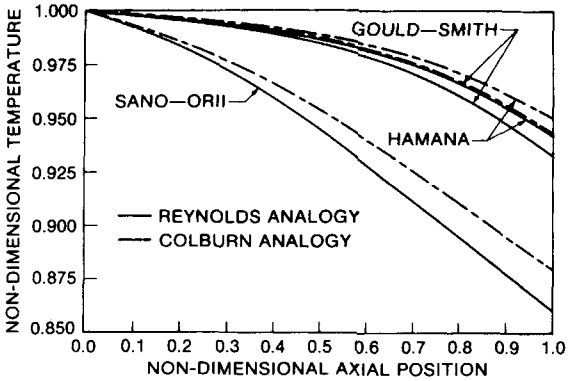

Fig. 2. Nondimensional fiber temperature vs. nondimensional axial position: (—) Reynolds analogy; (– -) Colburn analogy.

TABLE III
Heat Transfer Study: Reynolds vs. Chilton–Colburn Analogy (Convection Only)

	Sano–Orii		Hamana et al.		Gould-Smith	
Boundary layer analogy	Reynolds	Colburn	Reynolds	Colburn	Reynolds	Colburn
Drawing force (dyn)	159.02	153.65	144.14	143.95	144.38	144.11
Average Nusselt number	0.3366	0.2845	0.1283	0.1086	0.1483	0.1246
Average film coefficient[a]	269.13	201.36	71.19	56.69	87.39	68.38
Final temperature[b]	0.8606	0.8795	0.9418	0.9503	0.9333	0.9433

[a] Units are BTU/h · ft² · °F.
[b] Values expressed as fraction of initial temperature.

ber, which is less than unity, this correlation predicts a smaller value for the local Nusselt number than the Reynolds analogy which assumes that the Prandtl number is equal to 1. Thus, the Reynolds analogy predicts a lower temperature than when the Chilton–Colburn analogy is employed. Note that the results obtained using the Hamana et al. correlation and the Reynolds analogy are almost identical to those found with the Gould–Smith correlation and Chilton–Colburn analogy.

These results are summarized in Table III. It can be seen that the choice of either the Reynolds or Chilton–Colburn analogy has little effect on strand drawing force for each of the convection models employed in this study. Both the Gould–Smith and Hamana et al. correlations yield almost identical results for the drawing force while the original Sano–Orii correlation produces a force roughly 2.4% greater.

The effects of each of the models on strand shape and temperature are significant however. This is evident when one compares the range of the calculated average film coefficient, average Nusselt number, and final strand temperature.

Figures 3 and 4 show the results predicted by two additional convection models. Both the Kase–Matsuo correlation and the case of a constant film

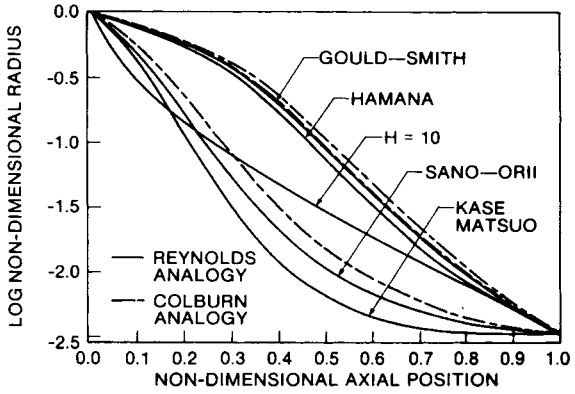

Fig. 3. Log nondimensional fiber radius vs. nondimensional axial position: (—) Reynolds analogy; (– -) Colburn analogy.

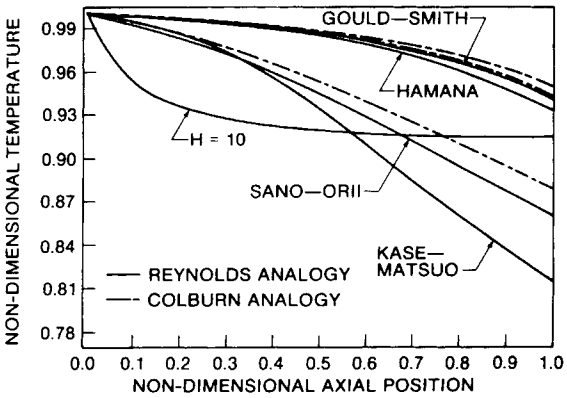

Fig. 4. Nondimensional fiber temperature vs. nondimensional axial position: (—) Reynolds analogy; (– -) Colburn analogy.

coefficient have been included. As mentioned previously, a value of $h = 10$ BTU/h · ft² · °F, estimated from McAdams,[23] was employed for this calculation.

The Kase–Matsuo correlation predicts greater cooling than any of the correlations based on skin friction. This correlation also follows the general trend of other models. The case of a constant film coefficient produces results which are quite different from the other calculations, however. This is most apparent when one examines the local temperature profiles.

The reason for the difference is easily accounted for when one considers that the assumption implied by using a constant film coefficient is that the thermal boundary layer is already fully developed at the tip exit. Since this is not true, the results calculated by assuming h is constant do not accurately represent the actual convection mechanism.

Table IV shows the results of the Kase–Matsuo correlation and a constant film coefficient as compared to the skin friction based correlations. In Table IV, the results of the models shown in Table III have been averaged to eliminate the effects of the boundary layer analogies for purpose of comparison.

TABLE IV
Heat Transfer Study: Convection Model Comparison

Correlation	Kase–Matsuo	Sano–Orii[a]	Hamana et al.[a]	Gould–Smith[a]	$h = 10$
Drawing force (dyn)	162.86	156.34	144.05	144.24	217.82
Average Nusselt number	0.4796	0.3106	0.1185	0.1365	0.1946
Average film coefficient[b]	512.00	235.25	63.94	77.89	10.0
Final temp[c]	0.8133	0.8701	0.9461	0.9384	0.9152

[a] Average results from Table III.
[b] Units are BTU/h · ft² · °F.
[c] Values expressed as fraction of initial temperature.

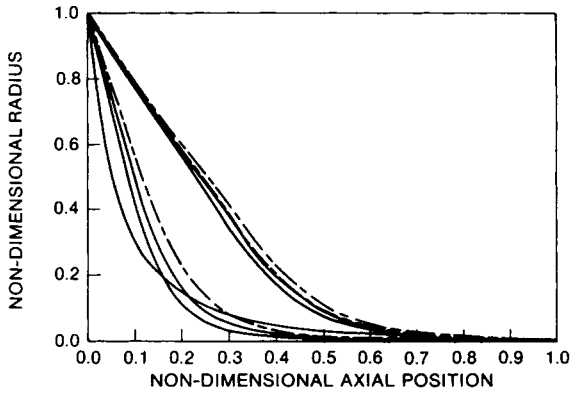

Fig. 5. Nondimensional fiber radius vs. nondimensional axial position.

These results show that there is very little difference in the calculated drawing force among the different convection models considered here. On the other hand, it is evident that large differences among the shapes, temperatures, Nusselt numbers, and local film coefficients result from each of the different correlations. Thus, the importance of employing an accurate convective film transfer coefficient in the calculations is clearly demonstrated.

Effects of Convection and Radiation

Up to this point, none of the reported results have included the effects of radiation. In Figures 5–8, the results for all of the convection models are presented, taking into account the radiation term by assuming a constant spectral emissivity of 0.30. The assumption of a constant emissivity may have to be modified to account for variations in spectral absorption and the other complications associated with radiation inside a participating media.

It is readily seen in these figures that radiation has a dramatic impact on shape, temperature, and drawing force. The most striking effect can be seen in Figures 5 and 6 which present the calculated shape of the jet for

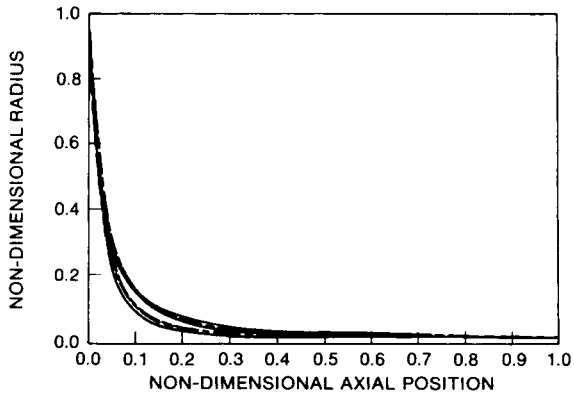

Fig. 6. Nondimensional fiber radius vs. nondimensional axial position.

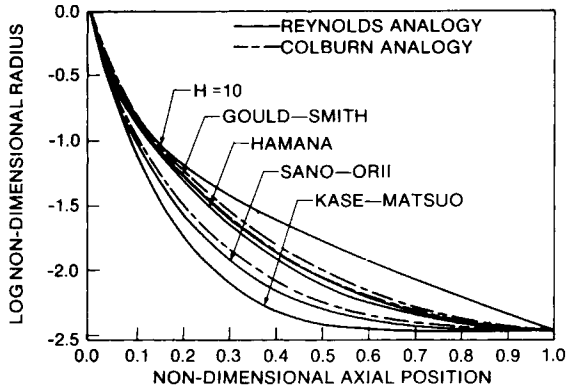

Fig. 7. Log nondimensional fiber radius vs. nondimensional axial position: (—) Reynolds analogy; (– -) Colburn analogy.

all of the convective models considered both with and without the effects of radiation.

Figures 7 and 8 present the calculated results for the radius and temperature as a function of position. These results are summarized in Tables V and VI.

The nonlinearity of the radiative heat transfer loss is most important in the upper region of the jet where the temperature is highest. This is because the radiative loss is proportional to the local temperature raised to the fourth power minus the local environment temperature raised to the fourth power.

This effect introduces a greater degree of cooling in the jet than possible by convection alone. Since the convection film coefficient (with the exception of h = const) is related to the local Reynolds number, the effect of the radiation is to decrease the fiber diameter locally, leading to an increase in the local velocity. This increases the local Reynolds number which in turn leads to larger values for both the local Nusselt number and film coefficient.

The drawing force is also increased roughly by 31–38% when the radiative cooling is included. This can be seen by comparing the results shown in

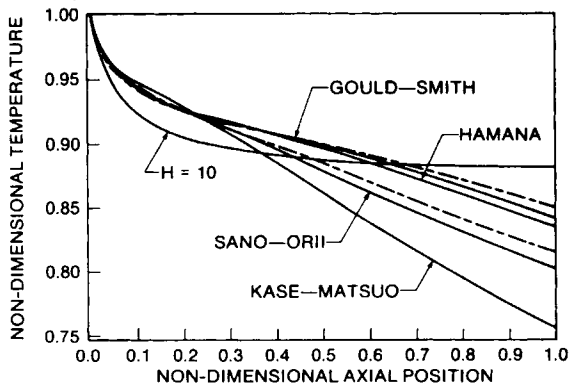

Fig. 8. Nondimensional fiber temperature vs. nondimensional axial position.

TABLE V
Heat Transfer Study: Reynolds vs. Colburn Analogy (Convection and Radiation[a])

Boundary layer analogy	Sano–Orii		Hamana et al.		Gould–Smith	
	Reynolds	Colburn	Reynolds	Colburn	Reynolds	Colburn
Drawing force (dyn)	361.68	351.89	319.02	315.03	322.89	318.29
Average Nusselt number	0.3853	0.3344	0.2159	0.1854	0.2454	0.1927
Average film coefficient[b]	402.54	329.83	199.41	162.95	237.89	192.56
Final temperature[c]	0.8015	0.8144	0.8418	0.8499	0.8340	0.8433

[a] $\epsilon = 0.30$.
[b] Units are BTU/h · ft² · °F.
[c] Values expressed as fraction of initial temperature.

Tables IV and VI. Radiation decreases the fiber diameter in a shorter axial distance than would be accomplished by convection alone. This results in a larger viscosity and greater drawing force.

Effects of Radiation

In order to assess the importance of radiation on strand shape and drawing force, another series of calculations were made. In these calculations, the effect of convection was eliminated and all cooling was assumed to take place by radiation only. The effects of radiative cooling were measured against an isothermal flow model calculated using the data shown in Table II.

Figures 9–11 present the results of the effects of different emissivities on shape and temperature as a function of position. It should be noted that small changes in emissivity can have a large influence on shape, temperature and drawing force. These effects are summarized in Table VII.

Figure 11 presents the drawing force as a function of emissivity. For values of emissivity smaller than 0.10, the effect of radiation upon force is nonlinear while for values of $\epsilon > 0.10$ the curve is almost linear.

TABLE VI
Heat Transfer Convection Models Including Radiative Cooling[a]

Correlation	Kase–Matsuo	Sano–Orii[b]	Hamana et al.[b]	Gould–Smith[b]	$h = 10$, $\epsilon = 0.30$
Drawing force (dyn)	372.41	356.78	317.03	320.59	397.75
Average Nusselt number	0.5642	0.3599	0.2007	0.2191	0.1100
Average film coefficient[c]	701.44	366.19	181.18	215.23	10.0
Final temp[d]	0.7553	0.8080	0.8459	0.8387	0.8805

[a] $\epsilon = 0.30$.
[b] Results averaged from Table V.
[c] Units are BTU/h · ft² · °F.
[d] Values expressed as fraction of initial temperature.

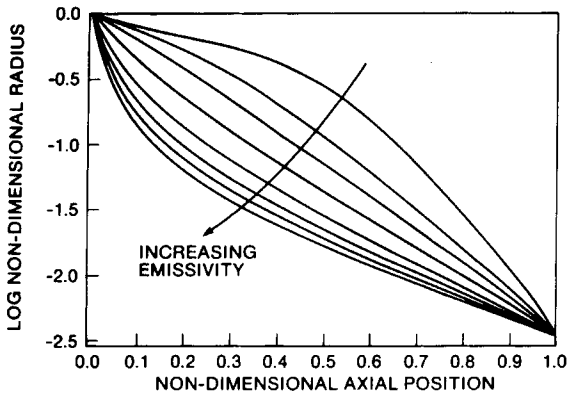

Fig. 9. Log nondimensional fiber radius vs. nondimensional axial position.

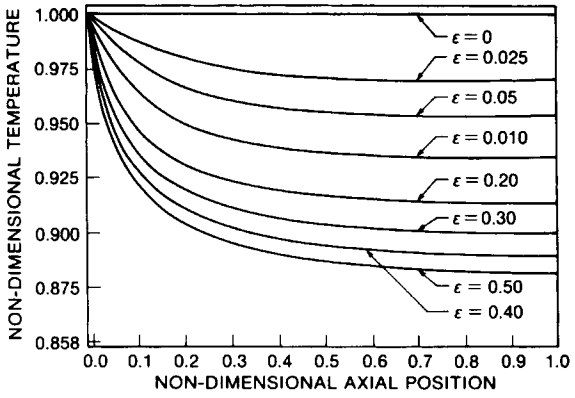

Fig. 10. Log nondimensional fiber temperature vs. nondimensional axial position.

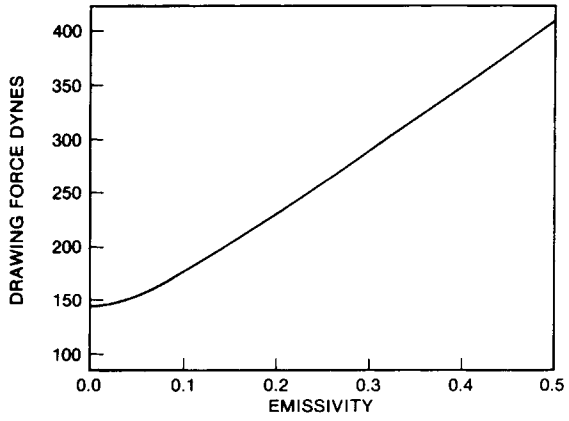

Fig. 11. Drawing force as a function of emissivity.

TABLE VII
Heat Transfer Study: Effects of Radiative Cooling Only

Emissivity	Drawing force (dyn)	Final temperature[a]
0	143.31	1.0000
0.025	146.93	0.9684
0.05	154.65	0.9520
0.10	177.38	0.9330
0.20	232.41	0.9114
0.30	291.11	0.8976
0.40	351.15	0.8874
0.50	411.85	0.8793

[a] Values expressed as fraction of initial temperature, which is 2100°F.

SUMMARY AND CONCLUSIONS

This study has presented the effects of heat transfer on melt-spinning processes. The results can be summarized as follows:

1. The use of a constant value to estimate the magnitude of the convective film transfer coefficient will lead to results that are inconsistent with our understanding of the physical process.

2. In the absence of any other information regarding the nature of the convective film coefficient, it is suggested that all studies be bound by using both the Kase–Matsuo and Gould–Smith correlations described in this paper because they provide an upper and lower bound for the drawing force. A realistic shape of the jet will be found somewhere between these bounds.

3. The effects of using either the Reynolds or Chilton–Colburn analogies upon the calculated drawing force are insignificant in the absence of radiation. They do have a significant effect upon both the shape and temperature profiles of the jet however. The Chilton–Colburn analogy tends to predict a larger strand temperature than the Reynolds analogy. In the presence of radiative cooling, these effects are of lesser importance because radiation is the dominant mode of heat transfer.

4. Radiative cooling is a dominant mode of heat transfer and is of particular importance in the upper jet region. Small changes in the spectral emissivity can lead to relatively large changes in drawing force.

Special acknowledgement is extended to Dr. Juan I. Ramos, Assistant Professor of Mechanical Engineering, Carnegie Mellon University, Pittsburgh, Pa., for his assistance in the development of the numerical methods used to implement the solution of the governing equations described in this paper.

References

1. L. R. Glicksman, PhD thesis, Mechanical Engineering Department, Massachusetts Institute of Technology, 1964.
2. H. Schlichting, *Boundary Layer Theory,* 7th ed., McGraw-Hill, New York, 1979.
3. M. B. Glauert and M. J. Lighthill, *Proc. Roy. Soc. London, Ser. A,* **230**, 188–203 (1955).
4. B. C. Sakiadis, *AIChE J.*, **7**, 467–472 (1961).
5. R. E. Sayles, PhD thesis, Division of Engineering, Brown University, 1982.
6. C. A. Moore and J. R. A. Pearson, *Rheol. Acta.,* **14**, 436–446 (1975).

7. D. E. Bourne and D. G. Elliston, *Int. J. Heat Mass Transfer*, **13**, 583–593 (1970).
8. F. T. Geyling, *14th International Congress of Theoretical and Applied Mechanics*, Delft, Netherlands, 1976 (unpublished).
9. J. L. White, *Polym. Eng. Rev.*, 1(4), 297–362 (1981).
10. S. Kase and T. Matsuo, *J. Appl. Polym. Sci.*, **3**, 2541–2554 (1965).
11. S. Kase and T. Matsuo, *J. Appl. Polym. Sci.*, **2**, 251–287 (1967).
12. Y. Sano and K. Orii, *Seni Gakkaishi*, **24**, 212 (1968).
13. I. Hamana, M. Matsui, and S. Kato, *Melliland Textil Brichte*, **50**, 382 (1969).
14. J. Gould and F. S. Smith, *J. Text. Inst.*, **72**, 38–49 (1980).
15. M. Matsui, *Trans. Soc. Rheol.*, **20**(3), 465–473 (1976).
16. F. P. Incropera and D. P. DeWitt, *Fundamentals of Heat and Mass Transfer*, McGraw-Hill, New York, 1972.
17. E. R. G. Eckert and R. M. Drake, *Analysis of Heat and Mass Transfer*, Wiley, New York, 1981.
18. M. A. Matovich and J. R. A. Pearson, *Ind. Eng. Chem. Fundam.*, **8**(3), 512–520 (1969).
19. L. R. Glicksman, *Trans. ASME*, Paper No. 68-FE-19.
20. M. M. Denn, in *Computational Analysis of Polymer Processing*, J. R. A. Pearson and S. M. Richardson, Eds., Applied Science, New York, 1983.
21. R. E. Maebius, PPG Fiber Glass Research Center, Pittsburgh, Pa., unpublished internal report, September 1983.
22. R. E. Maebius, PPG Fiber Glass Research Center, Pittsburgh, Pa., unpublished internal report, Decembr 1983.
23. W. H. McAdams, *Heat Transmission*, 3rd ed., McGraw-Hill, New York, 1954.

Received July 23, 1984
Accepted August 31, 1984